Journal of
Applied Remote Sensing

RemoteSensing.SPIEDigitalLibrary.org

Radiometric consistency between GOES-16 ABI and VIIRS on Suomi NPP and NOAA-20

Sirish Uprety
Changyong Cao
Xi Shao

SPIE.

Sirish Uprety, Changyong Cao, Xi Shao, "Radiometric consistency between GOES-16 ABI and VIIRS on Suomi NPP and NOAA-20," *J. Appl. Remote Sens.* **14**(3), 032407 (2020), doi: 10.1117/1.JRS.14.032407

Radiometric consistency between GOES-16 ABI and VIIRS on Suomi NPP and NOAA-20

Sirish Uprety,[a,*] Changyong Cao,[b] and Xi Shao[a]
[a]University of Maryland, CISESS, College Park, Maryland, United States
[b]NOAA/NESDIS/STAR, College Park, Maryland, United States

Abstract. NOAA has both geostationary (GEO) and polar orbiting (LEO) satellites that are procured through different vendors. For long-term environmental studies, it is essential to establish consistent radiometric calibration among satellite instruments irrespective of the satellite platforms. The Visible Infrared Imaging Radiometer Suite (VIIRS) onboard the Suomi National Polar-orbiting Partnership (S-NPP) and NOAA-20 satellites has been providing critical weather and climate-related data. With the launch of NOAA-20 in November 2017, the global coverage of VIIRS has doubled. With more than 7 years in space, S-NPP VIIRS has been rigorously calibrated and validated. We aim to quantify the radiometric consistency between the two VIIRS instruments through double differencing using GOES-16 Advanced Baseline Imager (ABI) as a reference instrument. We also provide insight into the temporal radiometric consistency between VIIRS and ABI. Since no direct simultaneous nadir overpasses (SNOs) exist between SNPP and NOAA-20 for intercomparison, GEO-LEO intercalibration is performed using SNOs between ABI and VIIRS instruments. We show that the NOAA-20 VIIRS measured top-of-atmosphere (TOA) reflectance is consistently lower than that of the S-NPP, mostly on the order of 2% to 3%, consistent with the past studies. GOES-16 ABI-observed reflectance is higher than both VIIRS instruments. SNOs over the all-sky tropical ocean are analyzed to quantify the bias for both NOAA-20 and S-NPP VIIRS relative to ABI. The impact on bias due to spectral differences is accounted for using spectral band adjustment factors estimated using hyperspectral measurements from SCIAMACHY. Uncertainties exist mainly due to calibration uncertainties in VIIRS and ABI, the time difference between the VIIRS and ABI observations, differences in cloud contamination, spectral response function differences, and lack of *in-situ* hyperspectral data to account for the spectral bias. [DOI: 10.1117/1.JRS.14.032407]

Keywords: VIIRS and ABI radiometric consistency; NOAA-20 VIIRS calibration; VIIRS RSB bias; double differencing.

Paper 190962SS received Dec. 6, 2019; accepted for publication May 11, 2020; published online May 29, 2020.

1 Introduction

It has been more than 7 years since the SNPP Visible Infrared Imaging Radiometer Suite (VIIRS) started collecting Earth observation data. Over the period, the sensor has been performing very well with continuous rigorous calibration and validation. The VIIRS Earth View observations have doubled since November 2017, after the launch of NOAA-20.

VIIRS has 13 reflective solar bands (RSBs), 1 day/night band, and 8 thermal emissive bands. The operational radiometric calibration for RSB is based on an onboard solar diffuser (SD)-based calibration system.[1] NOAA-20 VIIRS has gone through a few major look-up table updates during early launch, with the latest calibration update on April 27, 2018. Since then, the operational calibration gain has been kept constant due to the excellent stability of the instrument reported by multiple validation techniques including lunar trending. Several independent satellite instrument validation techniques, such as comparing VIIRS over well-characterized pseudo-invariant calibration sites (PICS), lunar time series, deep convective cloud trending (DCC),

*Address all correspondence to Sirish Uprety, E-mail: sirish.uprety@noaa.gov

1931-3195/2020/$28.00 © 2020 SPIE

intercomparison using simultaneous nadir overpass (SNO) over high latitude polar snow, extended SNO (SNOx) over low latitude Saharan desert and clear sky ocean, are used to evaluate the radiometric performance of VIIRS and give extensive information on instrument gain change (degradation) over time. Both SNPP and NOAA-20 VIIRS are continuously monitored to ensure that the radiometric accuracy and stability of the instruments are well within the specifications.[2–5] To use VIIRS data in long-term scientific applications and to establish a long-term data continuity of environmental data records, VIIRS calibration should be consistent and independent of the satellite platform.

GOES-16 was launched in November 2016 with Advanced Baseline Imager (ABI) as a major payload instrument on-board. ABI is a major advancement in instrumentation compared with previous GOES imager instruments in terms of Earth observation capabilities, such as higher frequency of Earth observation, presence of onboard calibration system for RSB, and high spatial resolution with more spectral bands. ABI has 16 bands with six solar reflective bands covering from 0.47 to 2.24 μm. Similar to VIIRS, ABI is equipped with an SD for six solar reflective bands calibration and a blackbody for 10 emissive bands calibration. Details on the ABI instrument can be found in earlier studies.[6–8] This study aims to evaluate the radiometric consistency between the two VIIRS instruments through double differencing using GOES-16 ABI. Both VIIRS instruments are compared with ABI over all-sky tropical ocean (ATO) to estimate the bias time series.

With two VIIRS sensors in space, it is necessary for them to be radiometrically consistent to establish long-term data continuity. The past study suggests that there exists near consistent radiometric bias between the two VIIRS sensors for RSBs.[9] The bias is mostly within 2% to 3%, with NOAA-20 observed top-of-atmosphere (TOA) reflectance being lower than SNPP VIIRS.[9] The past study was based on intercomparison of each VIIRS instrument with AQUA MODIS and then double differencing the bias trend.

Unlike NOAA-20, S-NPP VIIRS operational calibration has gone through a number of major updates in the sensor data records (SDR) algorithm and calibration parameters over the mission life. This has led to temporal inconsistencies in the radiometric calibration of the SDR products.[10,11] In addition, past studies have shown that some of the VIIRS RSB such as M5 (0.6 μm) and M7 (0.86 μm) suggest larger temporal bias when compared with other well-calibrated instruments such as AQUA MODIS and Landsat OLI.[2] To make VIIRS data more useful and reliable for time series studies, the entire SDR archive from January 2012 to March 2017 has been reprocessed at NOAA/STAR. However, this study uses nearly 1 year of VIIRS data (since July 2018) produced by NOAA operations (not the reprocessed data) and is readily available to users from CLASS. Since early 2017, S-NPP VIIRS operational calibration is consistent with no major calibration update. Unlike S-NPP, the NOAA-20 VIIRS instrument has been very stable since launch, and its postlaunch gain has not been updated since April 27, 2018. Any discontinuity in the VIIRS bias trending relative to ABI should result from ABI calibration updates. Still, after double differencing the VIIRS bias trends, the radiometric consistency trend among two VIIRS instrument should be smooth because the impact due to any calibration updates in GOES-16 ABI is cancelled out.

It is desirable to compare instruments over well-characterized homogeneous calibration targets to reduce uncertainties resulting from registration errors. Unlike LEO instruments (such as VIIRS and MODIS), GOES-16 ABI cannot view large homogeneous PICS sites in Saharan desert (such as Libya 4 desert) and Dome C site in Antarctica. Thus, the intercomparison has to rely on calibration sites such as Sonoran desert and SNOs in the tropical region. In addition, lunar trending and other techniques such as using the DCC to quantify the radiometric accuracy and stability have also been widely used.[12–14] Since ABI observes the full Earth disc every 10 min, multiple SNOs can happen with VIIRS every day. Comparing ABI with VIIRS using SNOs over ATO not only provides more datasets for analysis but also helps to establish the radiometric agreements over a wide dynamic range, from clear sky ocean to bright clouds. Radiometric consistency among the two VIIRS instruments is evaluated using the double differencing of the bias time series. VIIRS and ABI comparison helps to evaluate the temporal bias of NOAA-20 RSB relative to SNPP and quantifies the ABI radiometric performance over time. GOES-16 ABI and VIIRS intercomparison results using the ray-matching technique have been reported in the past.[15] In addition to SNO, radiometric validation of GEO instruments can also be

performed by comparing with other well calibration sensors over stable Earth calibration sites. One such study demonstrated this by comparing AHI with VIIRS over an Australian desert.[16]

In addition to the ATO-based comparison, the radiometric agreement between the two VIIRS instruments is also validated over a Saharan desert PICS. The two instruments are directly compared over the Libya 4 calibration site. Libya 4 is a widely used CEOS endorsed calibration site for analyzing the postlaunch radiometric performance of satellite sensors. VIIRS radiometric consistency analyzed over ATO involved double difference using ABI. The use of ABI can contribute to additional uncertainty in comparison. Whereas, directly comparing two VIIRS instruments over the Libya 4 makes the comparison simple and free of additional uncertainties from the reference instrument. However, this is under the assumption that the calibration site remains stable and does not change over time. In addition, the two VIIRS instruments observe the Libya 4 site at different days and time, which results in uncertainties due to the bidirectional reflectance distribution function (BRDF). Nonetheless, VIIRS relative radiometric bias estimated by trending and comparing the TOA reflectance over Libya 4 provides an opportunity to validate the VIIRS-ABI intercomparison result.

2 Intercomparison Methodology

GOES-16 ABI and VIIRS are compared for matching RSBs. The first six bands of ABI match with VIIRS over the region 0.4 to 2.2 μm as shown in Fig. 1 and Table 1. The figure shows that ABI bands 1 (0.47 μm) and 2 (0.67 μm) have the largest spectral differences with ABI being wider than VIIRS. Although the impact of spectral differences in intercomparison can be accounted for through the spectral band adjustment factor (SBAF), larger uncertainties can still exist due to the lack of *in-situ* hyperspectral measurements used in SBAF computation.

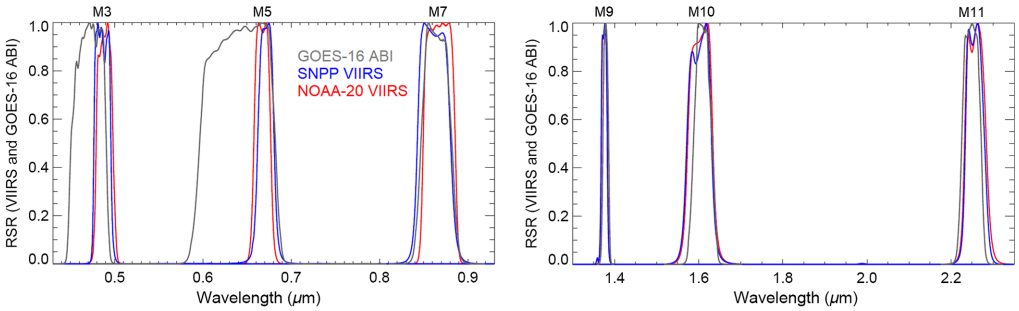

Fig. 1 RSRs for NOAA-20/SNPP VIIRS and GOES-16 ABI. Larger spectral differences can be observed for VIIRS bands M3 and M5.

Table 1 ABI bands with matching VIIRS bands.[17,18]

ABI		VIIRS		
Band	Resolution (km)	Matching band	Resolution (km)	Primary use
1 (0.47 μm)	1	M3 (0.488)	0.75	Daytime aerosol over land, coastal water mapping
2 (0.64 μm)	0.5	M5 (0.672)	0.75	Daytime clouds, fog, insolation, winds
3 (0.87 μm)	1	M7 (0.865)	0.75	Daytime vegetation, burn scar, aerosol over water, winds
4 (1.38 μm)	2	M9 (1.378)	0.75	Daytime cirrus clouds
5 (1.61 μm)	1	M10 (1.61)	0.75	Daytime clouds-top phase and particle size, snow
6 (2.25 μm)	2	M11 (2.25)	0.75	Daytime land, clouds properties, particle size, vegetation, snow

2.1 *VIIRS Calibration*

VIIRS onboard calibration system for RSBs consists of a full aperture SD that is illuminated by the Sun once per orbit at high latitudes in the Southern Hemisphere. An attenuation screen is used to avoid the saturation of the SD measurement. The BRDF of the SD and the transmittance of the attenuation screen are measured prelaunch and updated on-orbit using spacecraft yaw maneuver-based measurements. Given the angles of incidence, the reflected solar radiance can be computed and is used as a reference to produce calibrated reflectance and radiance. The space view (SV) provides the offset measurements needed for the calibration. The SD degradation is monitored by the solar diffuser stability monitor (SDSM) with detectors covering from blue to the near-infrared spectral range. It uses the Sun as the reference and views the Sun and the SD to determine the degradation of the SD, which in turn is used to compensate for the SD degradation in the onboard calibration. Details on the VIIRS instrument design and onboard calibration system can be found in Refs. 1 and 19. Exposing the SD to the Sun continuously has pros and cons. One positive side is that there is no mechanical door involved in the instrument, thus removing any chance of mechanical failure in the future. However, with continuous exposure to the Sun, the degradation in the SD is continuous and strong. Past study explains how the exposure to solar UV radiation and energetic particles leads to even faster degradation in the SD short wavelength and how the SD surface roughness-based Rayleigh scattering model can be used to explain the spectral-dependent degradation of the SD.[20] Thus, even with the presence of SDSM, it is challenging to quantify the SD degradation very accurately. This could possibly add small spurious and artificial corrections in the calibration. Studies in the past have shown that combining VIIRS onboard SD-based calibration along with lunar trending can result in optimal calibration stability better than 0.2%.[21]

The calibration equation for the Earth view data utilizes the F-factor, which is the multiplication factor or the inverse of the instrument gain. F-factors are computed for each band, detector, and gain stage and over each half-angle mirror (HAM) side[22] and are utilized in radiance calculation as

$$L = F \times (c_0 + c_1 \times d_n + c_2 \times d_n^2)/R_{\mathrm{RVS}}, \tag{1}$$

where c_0, c_1, and c_2 are calibration coefficients determined prelaunch that are temperature-dependent, R_{RVS} is the relative response versus the scan angle of the HAM, and d_n is the background (SV) subtracted detector measured Earth view digital counts. The F-factor is calculated as the ratio between the calculated at-aperture radiance of the SD using the specified solar model and the measured radiance based on SD counts.

2.2 *ABI Calibration*

This study uses nearly 1 year of GOES-16 ABI L1B data operationally calibrated and distributed by NOAA. The only major calibration adjustment for data during the period covered by this paper was performed for band 2, which was adjusted for large calibration bias[23] The ABI onboard calibration system for RSB consists of an SD called the solar calibration target (SCT) which is made of Spectralon. Unlike VIIRS, ABI does not have SDSM to monitor SD degradation. The VIIRS SD is continuously exposed to the Sun, unlike that of ABI. The ABI SCT is viewed frequently (e.g., every 2 days) during the first years after launch but is gradually changed to quarterly observations after the radiometric calibration is well characterized.[6] ABI SD degradation is small compared with that of VIIRS due to the low exposure rate. With the exposure to the Sun once every 3 months, the onboard calibration system may not be able to capture instrument-related anomalies and degradation that happens within the 3 months period during the absence of SD observations. This can directly impact the calibration stability, which in turn can result in poor SDR quality. In this study, the radiometric consistency between VIIRS is determined using the double difference of bias trends relative to ABI. Thus, the impact of long-term drifts in ABI calibration is cancelled out. However, the radiometric bias trends of each VIIRS instrument relative to ABI can clearly show any drifts present in ABI, assuming that the VIIRS is stable over the period. In addition to onboard SCT, GOES-16 ABI uses other techniques such as lunar observations to monitor instrument degradation.[6] Lunar-based degradation monitoring

cannot be implemented during early launch due to the insufficient number of measurements and needs a few years to build a time series with a reliable number of data points that is matured enough to characterize the instrument degradation.[5,21] With SD viewing every 3 months, it must be assumed that the instrument remains stable during the 3-month time period between the two SD observations. Like GOES-16 ABI, there are other instruments for which SD is not continuously exposed, such as Landsat 8 OLI. However, unlike ABI, OLI has two SDs, one of which is exposed to the Sun regularly on a weekly basis and the other pristine SD which is exposed twice a year to track the degradation of the primary (frequently exposed) SD.[24] With the absence of onboard SD degradation monitoring, it becomes more challenging and complicated to accurately characterize the temporal instrument degradation of ABI.

The radiance observed by GOES-16 ABI RSB channel viewing the Earth scene is determined from the measured counts (C) of the earth view (ev) and the space view (sv) as follows:

$$\langle L_{\mathrm{ev}} \rangle = \frac{M\Delta C_{\mathrm{ev}} + Q\Delta C_{\mathrm{ev}}^2}{\rho_{\mathrm{NS}}^{\mathrm{ev}}\rho_{\mathrm{EW}}^{\mathrm{ev}}}, \tag{2}$$

where $\langle L_{\mathrm{ev}} \rangle$ is the band-averaged spectral radiance for the scene in the Earth view, i.e., $\mathrm{W}/(\mathrm{m}^2\text{-sr-}\mu\mathrm{m})$ for the RSB. ΔC_{ev} is the count difference between the Earth view and SV, i.e., $\Delta C_{\mathrm{ev}} = C_{\mathrm{ev}} - C_{\mathrm{sv}}$. $\rho_{\mathrm{NS}}^{\mathrm{ev}}, \rho_{\mathrm{EW}}^{\mathrm{ev}}$ and Q are the linear and quadratic coefficients, respectively. The quadratic coefficient Q is first determined prelaunch per band and per detector element and later updated postlaunch. The linear coefficient M for RSB is determined on-orbit by observing the SD. The $\rho_{\mathrm{NS}}^{\mathrm{ev}}, \rho_{\mathrm{EW}}^{\mathrm{ev}}$ are the reflectance of the east/west and north/south scan mirrors, respectively, when viewing the Earth scene. Unlike VIIRS, the ABI calibration coefficients do not account for the temperature variation in the focal plane and electronics.

2.3 *Intercomparison*

NOAA-20 and SNPP VIIRS can be compared with GOES-16 ABI over low latitude SNOs. ABI has been collecting full disc Earth imagery every 15 min since launch (changed to 10 min from April 2, 2019); thus, SNOs within 7.5 happen every day. However, the overlapping region used for comparison during SNOs can have large differences in solar and sensor geometry; thus, a large number of SNOs might get excluded mainly due to not meeting the matching criteria. GOES-16 ABI TOA reflectance is compared with each VIIRS instrument onboard SNPP and NOAA-20 to derive the bias trends. The bias indicates ABI radiometric performance relative to VIIRS. The trends show how well the ABI measurements agree with VIIRS. In addition, through double differencing, the difference between the individual VIIRS bias trends can be estimated; this represents the VIIRS radiometric consistency among each other. The intercomparison methodology used in this paper is based on past studies that have detailed descriptions of how the GOES data are compared with polar-orbiting instruments such as AQUA MODIS using ray matching.[13,25–27] The detailed steps used in intercomparison are given below.

2.3.1 *Identify SNO events and collect ABI and VIIRS data*

GOES-16 is in geostationary orbit, and hence SNOs exist with both SNPP and NOAA-20 every day.[28] Methodology on how SNOs can be predicted can be found in an earlier study.[29] Nearly three VIIRS orbits overlap with GOES-16 ABI during the daytime. One SNO event has VIIRS orbit closer to ABI nadir whereas the other two SNO events happen at higher scan angles. To reduce the impact due to the BRDF, the intercomparison of VIIRS with ABI at higher scan angles needs careful consideration of solar and sensor geometry differences. For each SNO, VIIRS and ABI data are collected. Both VIIRS and ABI can be downloaded from NOAA CLASS.[30] For each SNO event, VIIRS and ABI data with a time difference of <15 min are collected. GOES-16 ABI image selected for comparison has a time difference of <7.5 min since either the preceding or the following GOES image can be used. For each SNO, multiple VIIRS granules are collected for comparison. This study compares nearly 1 year of VIIRS data with ABI starting from July 2018.

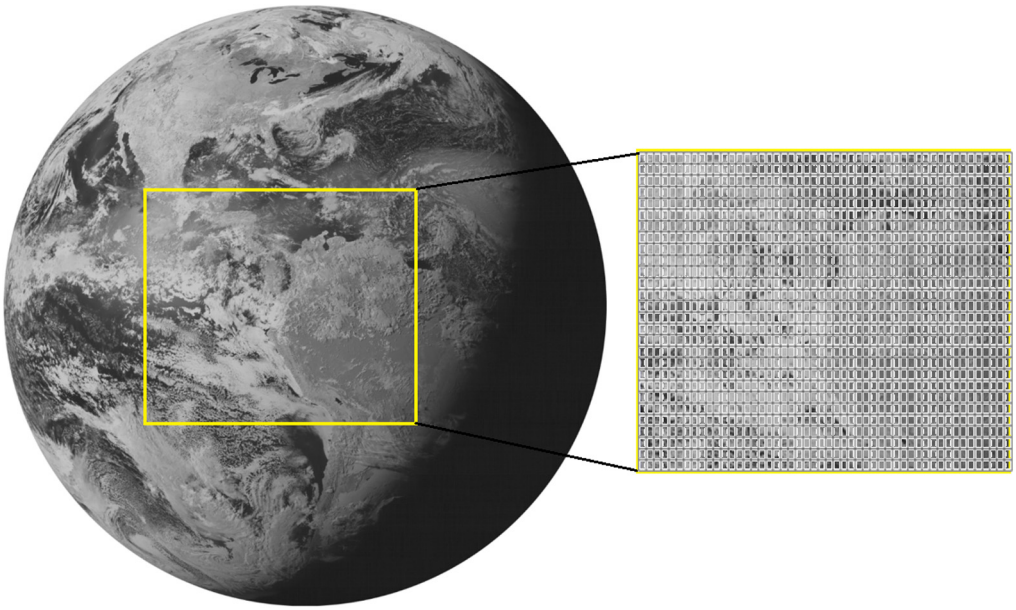

Fig. 2 ROI used in the intercomparison.

2.2.2 *Define ROI and perform the comparison*

Region of interest (ROI) for each SNO is defined as a rectangular region ranging ± 20 deg latitude and ± 20 deg longitudes from the center of the GOES-R subsatellite location (0 deg, -75 deg) as shown in Fig. 2. Each ROI is then divided into 0.5 deg $\times$ 0.5 deg bins in both the latitude and the longitude directions. ABI and VIIRS are compared over each bin, and the average over all of the valid bins for a given SNO provides the bias estimation. Multiple VIIRS granules collected during each SNO event are merged to get the VIIRS track length that covers the vertical boundary of the large ROI.

2.2.3 *Ray matching*

Ray matching is a widely used technique in GEO-LEO intercalibration.[13,25–27] A past study[13] describes how the technique has been used to transfer the Aqua MODIS calibration to all of the geostationary (GEO) imagers, resulting in the derivation of consistent fluxes and cloud retrievals over multidecadal Earth observation. Although the ray-matching-based calibration algorithm can be used to calibrate an instrument traceable to a reference instrument,[13] it has been used in this study to perform the intercomparison between the VIIRS and ABI using calibrated TOA reflectance. Ray matching is obtained between the two instruments based on the following criteria:

(a) Solar zenith angle difference: <5
(b) Viewing zenith angle difference: <15
(c) Relative azimuth difference: <15
(d) Spatial uniformity: <70%
(e) Exclude land
(f) Exclude sunglint
(g) Exclude views from direct backscatter (RAA > 170) or forward scatter (RAA < 10).

2.2.4 *Bias estimation*

For each 0.5 deg $\times$ 0.5 deg bin, with valid ray-matching criteria, bias can be computed for SNPP VIIRS relative to ABI and NOAA-20 VIIRS relative to ABI. Bias over all of the valid bins can be averaged to estimate bias for each SNO. However, to improve the weighted sampling over a dynamic range, observed bias values have been computed every week. All of the bias

Table 2 SCIAMACHY-based SBAF for SNPP and NOAA-20 VIIRS bands relative to matching GOES-16 ABI bands.

ABI bands	B1 (0.47 μm)	B2 (0.64 μm)	B3 (0.86 μm)	B4 (1.37 μm)	B5 (1.61 μm)	B6 (2.2 μm)
ABI/VIIRS (SNPP)	1.022	0.978	1.002	1.017	1.017	—
ABI/VIIRS (NOAA-20)	1.024	0.978	0.999	1.014	1.010	—

values estimated using SNOs processed every week are averaged to come up with a weekly bias value. The temporal trend of bias indicates the radiometric performance of ABI relative to VIIRS. In addition, the difference between the two bias trends suggests the radiometric consistency between the two VIIRS instruments.

2.2.5 *Spectral bias*

The impact due to spectral differences is accounted for using the SBAF. SBAF values for ATO are based on SCIAMACHY observations and are available at Ref. 31.[32] The ATO is used to get the SBAF values for each ABI and VIIRS matching band. Although the footprint size is large for SCIAMACHY (30 km $\times$ 60 km) that can closely represent the ATO scenario, the lack of *in situ* measurements adds uncertainties in estimated SBAF values. The uncertainties can be larger for ABI bands 1 and 2 due to larger spectral mismatch with VIIRS. Each SNO can have few valid 0.5 deg $\times$ 0.5 deg bins, and it is possible that the bins within one SNO event do not truly represent the all-sky ocean scenario. The valid bins in an SNO can be mostly cloudy or mostly clear sky or a uniform combination of cloud and clear sky pixels. In addition, some bins can be largely affected by cloud shadow. In such cases, spectral bias estimation from SCIAMACHY may not necessarily be accurate for each SNO-based bias. Thus, the study uses an average value of all of the bias values derived over a week from many SNOs. A single bias value computed for each week is a closer representation of all-sky ocean; thus, the SBAF from SCIAMACHY can be more reliably used in the study (Table 2).

2.2.6 *VIIRS radiometric consistency validation*

The SNPP and NOAA-20 VIIRS radiometric consistency derived using ABI through double differencing can be validated using PICS. PICS have been widely used among remote sensing communities to study the radiometric performance of satellite sensors. Saharan desert calibration sites have been used to characterize the sensor performance for more than a decade.[3,33–35] PICS can be used reliably to analyze the radiometric performance of the instruments as long as the sites have been rigorously characterized to ensure long-term stability. This paper uses Libya 4 desert (28.55° N, 23.39° E) shown in Fig. 3; the Committee on Earth Observation Satellites endorsed

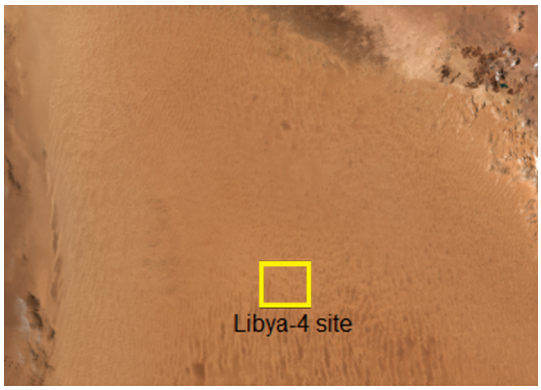

Fig. 3 Libya 4 calibration site.

the calibration site to perform postlaunch validation of satellite instruments such as VIIRS. The following steps summarize how data processing is performed for each band:

(a) For each nadir overpass of the satellite, an ROI of size 30 km × 30 km is extracted such that the center of the ROI has the same latitude and longitude as defined for each site in the earlier section.
(b) Each ROI needs to be checked for several clear-sky filtering criteria. Only the ROI with all clear sky pixels are considered for analysis. Cloud mask products from VIIRS are used to determine the level of cloud contamination.
(c) A spatial uniformity test is also performed such that the given ROI is considered valid only if its spatial uniformity (ratio of 1 standard deviation to mean reflectance) is better than 4%. This helps to filter out the majority of the cloud-contaminated observations including events such as sandstorms and heavy aerosols.
(d) In addition, a threshold of ±6- deg sensor zenith for all pixels within an ROI is used to limit the analysis only within nadir. After an ROI passes all of the above conditions, the mean and standard deviation are calculated, and a temporal trend is generated for each instrument. All data analysis is performed using at-sensor TOA reflectance.
(e) Steps (a) to (d) are performed for both SNPP and NOAA-20 VIIRS to generate the TOA reflectance time series.
(f) SBAF values are applied on NOAA-20 VIIRS to correct the systematic bias between the two VIIRS instruments resulting from the spectral differences between the two instruments. SBAF is computed using EO-1 Hyperion data (Table 3). The 1-sigma uncertainty in SBAF using Hyperion is <0.5% except for the cirrus band (3%). Scaling by SBAF converts NOAA-20 VIIRS reflectance to matching SNPP VIIRS band relative spectral response (RSR) equivalent.

3 Results and Discussion

The two VIIRS instruments are compared with GOES-16 ABI for nearly 1 year to establish the bias time series. The bias time series can be estimated using each SNO (Fig. 4) or by averaging over a fixed time period (Fig. 7). Sections 3.1 to 3.3 analyze the bias time series of each VIIRS relative to ABI. The difference between the two bias time series (one for each VIIRS instrument) suggests the radiometric consistency between the VIIRS.

Table 3 SCIAMACHY and EO-1 Hyperion-based SBAF for NOAA-20 VIIRS relative to SNPP. SNPP equivalent of NOAA-20 VIIRS reflectance = (NOAA-20 VIIRS reflectance) × SBAF.

SBAF	M3 (0.48 μm)	M5 (0.67 μm)	M7 (0.86 μm)	M9 (1.38 μm)	M10 (1.61 μm)	M11 (2.25 μm)
ATO (SCIAMACHY)	0.998	1.003	0.992	0.999	0.997	—
Libya 4 desert (Hyperion)	1	1.014	0.995	0.986	0.997	1.003

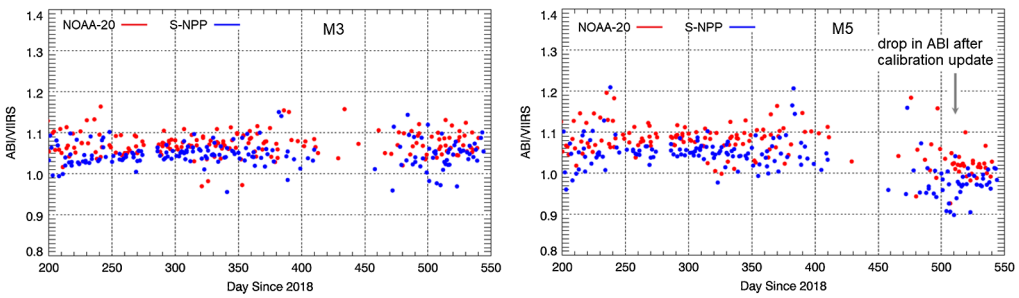

Fig. 4 The ratio of ABI (bands 1 and 2) and VIIRS over SNPP and NOAA-20.

3.1 *VIIRS and ABI Comparison*

Figure 4 shows the observed bias time series for NOAA-20 VIIRS relative to GOES-16 ABI. Each point in the plot represents one SNO event that represents an instantaneous event. Each SNO can have a different number of bins and different amounts of cloud and clear sky pixels resulting in large scatter in temporal trend. There exists a gap of nearly two months (near 450 days since 2018). The gap is mainly due to a lack of ABI and VIIRS bins satisfying the ray-matching criteria. The majority of the bins during this period have Sun glint angles lower than the allowed threshold. In addition, a large drop in ABI band 2 can be seen in the figure; this is due to a major calibration update in early April 2019.[36] For ABI band 2, bias result is consistent with the earlier studies that suggested that the ABI band 2 calibration was biased high by more than 6%.[37] Hence, the calibration update was intended to correct the overestimation in band 2 absolute calibration. A nearly 6% drop in ABI reflectance can be observed after the update.

For all-sky ocean, the dynamic range can extend from low reflectance clear sky ocean to high reflectance bright clouds. Hence, it is necessary to understand how the bias behaves over the large dynamic range and how that impacts the analysis. Figure 5 shows the ratio of ABI and VIIRS as a function of VIIRS reflectance. Bias at the lower reflectance range indicates large scatter. There could be multiple reasons behind nonlinear behavior at low reflectance, such as (a) nonlinearity in the instrument, (b) larger uncertainty in calibration at the lower end of the dynamic range, (c) spectral differences between the two instruments, (d) changing target reflectance due to a varying number of water and cloud pixels including different types of clouds for VIIRS resulting from time difference in observations, and (e) low signal-to-noise ratio for ABI at low radiance. To quantify the bias more accurately, the lower end of reflectance has been excluded. Thresholds were used such that for ABI bands 1 and 2, reflectance below 20% is excluded. Similarly, for bands 3, 5, and 6, reflectance below 10% is excluded from the analysis.

Figures 4 and 5 show a large scatter in the observed reflectance ratio between ABI and VIIRS. Each data point in Fig. 4 represents the averaged ratio over all of the bins (0.5 deg × 0.5 deg latitude and longitude) for each SNO event. Similarly, each data point in Fig. 5 shows the ratio of ABI and VIIRS for individual bins (0.5 deg × 0.5 deg latitude and longitude).

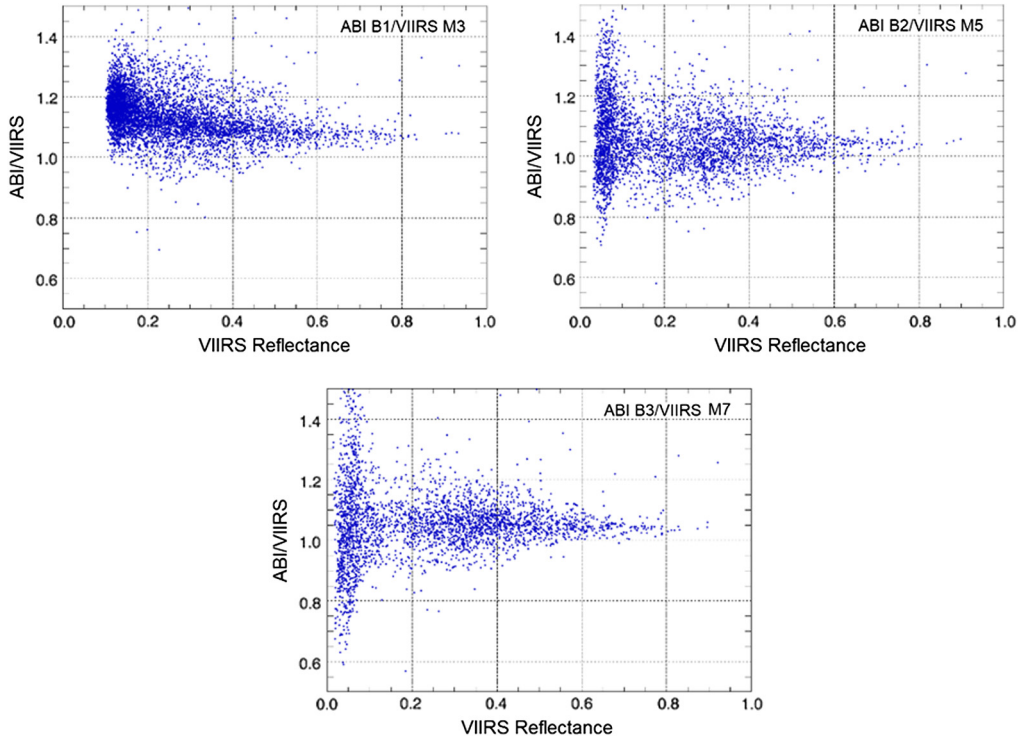

Fig. 5 ABI/VIIRS ratio as a function of VIIRS reflectance showing large scatter at low reflectance for ABI bands 1 to 3. Each data in the figure represents one bin (0.5 deg × 0.5 deg latitude/longitude). Data from entire period of analysis are shown.

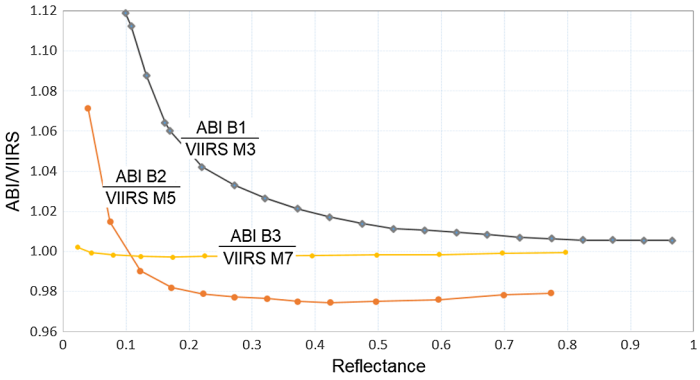

Fig. 6 SBAF changing with the reflectance. Reflectance changes due to the change in target spectra caused by varying cloud contamination. Reflectance for both VIIRS and ABI is obtained by convolving with SCIAMACHY spectra.

Although ABI and VIIRS are collocated for each bin, it is not necessary that both instruments view the identical target. This is because the all-sky ocean target is a mixed pixel between the ocean and the cloud. The time difference in observation by VIIRS and ABI by a few minutes can cause the movement in clouds and the change in solar/sensor geometry that results in increased uncertainty in the comparison. However, a major source causing the large scatter, and hence the larger uncertainty in the reflectance ratio could be due to the variation in spectral signature from bin to bin. This impact has been reduced by computing an average bias value over all of the bins for a given SNO. However, the number of bins and the location of valid bins can vary over SNOs. Since each bin can have a different level and type of cloud, the spectral signature can vary widely over the bins. Thus, the variation in the spectral signature can directly lead to larger scatter in the reflectance ratio. Figure 6 shows the ratio of ABI and VIIRS convolved SCIAMACHY spectra over varying all-sky ocean TOA reflectance. The chart attempts to simulate the variation in reflectance over ATO with a large dynamic range covering from clear sky ocean pixels to bright clouds. The figure shows the ratio between ABI and VIIRS over the first three ABI bands as a function of varying reflectance. ABI band 1 indicates a large spectral bias ranging from nearly 12% at 10% reflectance level (mostly clear sky ocean) to nearly 0.5% at 80% reflectance (bright clouds). A sharp increase in VIIRS M3 bias relative to ABI band 1 at low reflectance (Fig. 5) matches the spectral bias trend at low reflectance although the magnitude of the spectral bias is smaller. Accounting for the spectral bias as a function of reflectance could help to reduce the large uncertainty in VIIRS bias at low reflectance. For ABI band 2, although the spectral bias trend looks similar to band 1 showing nearly 9% variation, the large scatter at low reflectance (Fig. 5) cannot be explained well with the spectral bias trend. Similarly, for ABI band 3, the spectral bias trend as a function of reflectance is nearly flat due to closely matching RSRs, and hence the large scatter in bias at low reflectance cannot be explained with the flat trend. ABI bands 1 and 2 have a large spectral mismatch with VIIRS, and hence the spectral bias changes drastically over the large dynamic range. For ABI bands 1 and 2, accounting for the spectral difference as a function of reflectance improves the intercomparison result. Although this study uses a single SBAF value to correct for all SNOs, the impact due to spectral-dependent target spectra has been further reduced by averaging all SNOs over a week. Averaging over a longer period (weekly in this study) helps to obtain a nearly uniform sampling of data over a wider dynamic range. This reduces uncertainty due to variation in target spectral differences. This study uses about a year of ABI/VIIRS data, and hence the bias analysis is performed using weekly averaging. The larger uncertainty in spectral bias at low reflectance is the reason that the reflectance threshold of 0.2 and 0.1 are used in intercomparison. The use of reflectance threshold brings the SBAF curve to a more stable region; thus, using a single SBAF value for each band can still be reliable.

3.2 *VIIRS Radiometric Consistency*

As observed in Fig. 4, the bias values are largely scattered. The major reason could be due to the nonuniform sampling of data over the dynamic range for each SNO. Thus, this study uses a

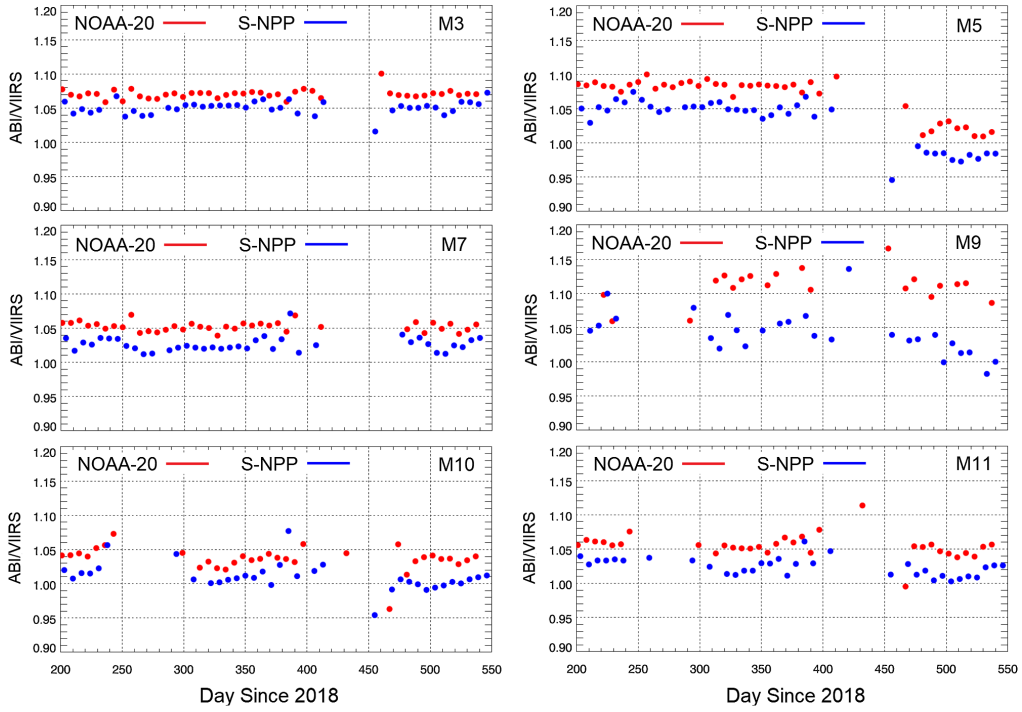

Fig. 7 ABI/VIIRS ratio showing (a) the ABI bias relative to each VIIRS instrument and (b) radiometric consistency between the VIIRS instruments onboard SNPP and NOAA-20.

weekly average to build a temporal bias trend for both SNPP and NOAA-20 VIIRS relative to ABI. Figure 7 shows the temporal trend of the ratio between ABI and VIIRS. The ratio takes into account the spectral differences between ABI and VIIRS. The figure suggests that ABI TOA reflectance is higher than VIIRS for all six matching ABI bands. The bias trends suggest that ABI-calibrated TOA reflectance agrees with SNPP VIIRS to within 5% for all bands. ABI band 1 indicates the largest bias of 5%. The rest of the bands including ABI band 2 (after ABI calibration update in April 2019) agree better to mostly within 2% except the cirrus band.

The bias between the two VIIRS instruments can be observed in Fig. 7. Each data point in the chart is computed by averaging the ratio between ABI and VIIRS values over a week. The past study by[9] suggested that the NOAA-20 VIIRS measured TOA reflectance is lower than the SNPP VIIRS by 2% to 3%, consistent with the result shown in Fig. 7. Bias trends for ABI bands 1, 2, and 3 are more stable than that for the rest of the bands. Although the bias for bands 4 to 6 is noisier, NOAA-20 VIIRS can still be observed to be lower than the SNPP VIIRS. The figure shows that the SNPP bias trends are more scattered than that of NOAA-20. Table 4 shows the NOAA-20 VIIRS bias relative to SNPP. Bias values are estimated based on linear fit to each time series. Bands M5 and M7 show a smaller bias (~3%) compared with an earlier study[9] that suggested more than 4%. The possible reason for this could be the larger uncertainty in spectral bias resulting from larger spectral mismatch and lack of *in situ* SCIAMACHY measurements used to compute SBAF. Band 4 is a cirrus band and has larger uncertainty in bias (3.5%), indicated by

Table 4 NOAA-20 bias values relative to SNPP.

NOAA-20 VIIRS bias	M3 (0.48 μm)	M5 (0.67 μm)	M7 (0.86 μm)	M9 (1.38 μm)	M10 (1.61 μm)	M11 (2.25 μm)
Using double difference with ABI	−2% ± 1.2%	−3.5% ± 1.3%	−2.8% ± 1.1%	−5.2% ± 3.5%	−2.5% ± 2.1%	−2.9% ± 1.8%
Libya 4 site	−1.86 ± 0.69%	−3.48 ± 0.47%	−3.45% ± 0.58%		1.49% ± 0.54%	−0.8% ± 2.0%

the largest scatter in data. The bias trends are not flat, and it is desirable to have a longer time series to statistically derive more accurate bias values.

3.3 *VIIRS Radiometric Consistency Validation over Libya 4 Calibration Site*

Sections 3.1 and 3.2 discussed the radiometric consistency between ABI with VIIRS and between the two VIIRS instruments. The radiometric agreement between the two VIIRS instruments derived using double differencing with ABI is validated using the Libya 4 calibration site. Figure 8 shows nearly 1 year of TOA reflectance trends of NOAA-20 and SNPP VIIRS over the Libya 4 site. Each point represents the average reflectance over a clear sky ROI of 30×30 km. Although SNPP VIIRS has a longer reflectance time series, only the data starting from 2018 is plotted to match the time period with NOAA-20. Longer time series for both instruments would be desirable for more accurate bias analysis and residual degradation characterization. Data are collected near nadir with a 16-day repeat cycle. However, there exists a gap over a certain period mainly due to the presence of cloud. Since the RSRs from the two VIIRS bands are not identical, the impact due to spectral differences is accounted for in the comparison. The spectral characteristics of the Libya 4 site have been characterized in the past.[2] The TOA reflectance time series shown in Fig. 8 has NOAA-20 VIIRS scaled using EO-1 Hyperion-based SBAF to match the response with the SNPP VIIRS RSR. Although the impact due to spectral differences is reduced after scaling, the uncertainties exist mainly due to the lack of *in situ* measurements and the low spectral resolution of Hyperion.

The figure shows that observed reflectance for NOAA-20 VIIRS is lower than that of SNPP, which is consistent with the double differencing-based bias estimated using ABI (Fig. 7). Band M3 and M11 are shown to have noisier time series compared with the other bands. Table 4 shows the NOAA-20 VIIRS bias relative to S-NPP. NOAA-20 M3 relative to SNPP is on the order of 2% or less. M5 and M7 indicate a larger bias of nearly 3.5%. This is mainly due to the

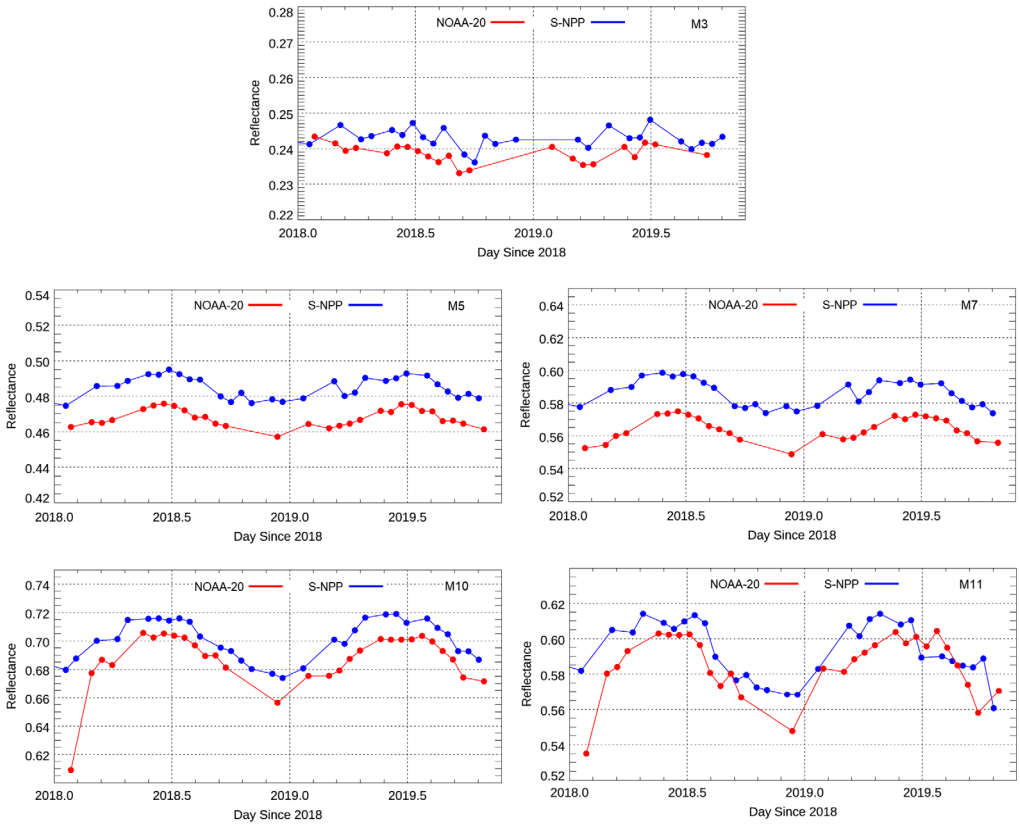

Fig. 8 NOAA-20 and SNPP VIIRS TOA reflectance comparison over Libya 4 for matching ABI bands 1 to 3, 5 and 6.

overestimation in absolute calibration of SNPP VIIRS as discussed in earlier studies.[2,3,9] Similarly, M10 and M11 suggest a 1% to 2% lower reflectance than SNPP VIIRS. Although the S-NPP and NOAA-20 satellites are 50 min apart, the local equatorial crossing time is nearly same. Each instrument views the Libya 4 site at nadir (the difference in sensor zenith is a fraction of a degree) exactly 8 days apart at the same local time (~11:30). The difference in solar zenith angle during the observation by the two instruments is mostly on the order of 0.5 deg to 1 deg. The impact due to the BRDF on bias is mostly on the order of 0.15%. This impact due to the BRDF has not been accounted for in bias calculation mainly due to two reasons. First, given the uncertainty level on the order of 0.5% or more over desert, this impact is minimal. Second, the Libya 4 site is used for validating the VIIRS radiometric consistency derived using ABI, which has uncertainty larger than 1%.

4 Conclusion

This study performed GOES-16 ABI and NOAA-20/SNPP VIIRS intercomparison using the ray-matching technique. The TOA reflectance data were compared over ATO to derive bias time series. The study analyzed the radiometric consistency between the two VIIRS instruments using weekly bias time series relative to GOES-16 ABI. It was found that the estimated bias values of NOAA-20 VIIRS relative to S-NPP mostly agree with the earlier study,[9] ranging from 2% to 3%. However, bands M5 (0.672) and M7 (0.865) indicated a slightly smaller bias than that from the past study by nearly 1%. The reason could be mainly due to the spectral differences and the uncertainty in the spectral bias derived from SCIAMACHY. The study also revealed the impact of a larger RSR mismatch in comparison due to variation in spectral signatures among the ROI bins. The ATO ray-matching methodology employed here can create spectral biases by more than 10% for low reflectance conditions. Further ATO SBAF enhancements, such as reflectance-dependent SBAFs, would greatly reduce this bias. The study also suggested that ABI is consistent with SNPP VIIRS to within 5% for band 1 and within 2% for the rest of the bands except the cirrus band. The paper provides important information to the user community on radiometric consistency between GOES-16 ABI and NOAA-20/SNPP VIIRS. Consistent radiometric calibration among the satellite sensors is a key requirement in long-term environmental studies.

Acknowledgments

The paper contents are solely the opinions of the authors and do not constitute a statement of policy, decision, or position on behalf of NOAA or the U.S. government.

References

1. C. Cao et al., "Early on-orbit performance of the visible infrared imaging radiometer suite onboard the Suomi national polar-orbiting partnership (S-NPP) satellite," *IEEE Trans. Geosci. Remote Sens.* **52**(2), 1142–1156 (2014).
2. S. Uprety and C. Cao, "Suomi NPP VIIRS reflective solar band on-orbit radiometric stability and accuracy assessment using desert and Antarctica Dome C sites," *Remote Sens. Environ.* **166**, 106–115 (2015).
3. S. Uprety et al., "Radiometric intercomparison between Suomi-NPP VIIRS and aqua MODIS reflective solar bands using simultaneous nadir overpass in the low latitudes," *J. Atmos. Oceanic Technol.* **30**(12), 2720–2736 (2013).
4. C. Cao et al., "Suomi NPP VIIRS sensor data record verification, validation, and long-term performance monitoring," *J. Geophys. Res.* **118**, 11,664–11,678 (2013).
5. T. Choi et al., "Radiometric stability monitoring of the Suomi NPP visible infrared imaging radiometer suite (VIIRS) reflective solar bands using the Moon," *Remote Sens.* **8**(1), 15 (2016).
6. S. Kalluri et al., "From photons to pixels: processing data from the advanced baseline imager," *Remote Sens.* **10**(2), 177 (2018).

7. F. Yu et al., "Early radiometric calibration performances of GOES-16 Advanced Baseline Imager," *Proc. SPIE* **10402**, 104020S (2017).
8. T. J. Schmit et al., "A closer look at the ABI on the GOES-R series," *Bull. Am. Meteorol. Soc.* **98**(4), 681–698 (2017).
9. S. Uprety et al., "Evaluating NOAA-20 and S-NPP VIIRS radiometric consistency," *Proc. SPIE* **10781**, 107810V (2018).
10. S. Uprety, C. Cao, and S. Blonski, "Retrospective analysis of Suomi NPP VIIRS radiometric bias for reflective solar bands due to operational calibration changes," *Int. J. Remote Sens.* **37**(22), 5472–5489 (2016).
11. S. Blonski and C. Cao, "Suomi NPP VIIRS reflective solar bands operational calibration reprocessing," *Remote Sens.* **7**(12), 16131–16149 (2015).
12. D. Doelling et al., "Geostationary visible imager calibration for the CERES SYN1deg edition 4 product," *Remote Sens.* **10**(2), 288 (2018).
13. D. R. Doelling et al., "Improvements to the geostationary visible imager ray-matching calibration algorithm for CERES Edition 4," *J. Atmos. Oceanic Technol.* **33**(12), 2679–2698 (2016).
14. F. Yu and X. Wu, "Radiometric inter-calibration between Himawari-8 AHI and S-NPP VIIRS for the solar reflective bands," *Remote Sens.* **8**(3), 165 (2016).
15. S. Uprety, C. Cao, and X. Shao, "Geo-Leo intercalibration to evaluate the radiometric performance of NOAA-20 VIIRS and GOES-16 ABI," *Proc. SPIE* **11127**, 111270S (2019).
16. T. Chang et al., "GEO-LEO reflective band intercomparison with bidirectional reflectance distribution function and atmospheric scattering corrections," *J. Appl. Remote Sens.* **12**(1), 014002 (2018).
17. "GOES-R series product definition and users' guide, Volume 3: Level 1B products. Geostationary operational environmental satellite, R series (goes-r) core ground segment," contract no: dg133e-09-cn-0094, document control number: 7035538, CDRL SE-16, revision G (2018).
18. VIIRS ATBD, "Joint polar satellite system (JPSS) visible infrared imaging radiometer Suite (VIIRS) sensor data records (SDR) algorithm theoretical basis document (ATBD)" (2013).
19. N. Lei, Z. Wang, and X. Xiong, "On-orbit radiometric calibration of Suomi NPP VIIRS reflective solar bands through observations of a sunlit solar diffuser panel," *IEEE Trans. Geosci. Remote Sens.* **53**(11), 5983–5990 (2015).
20. X. Shao, C. Cao, and T. C. Liu, "Spectral dependent degradation of the solar diffuser on Suomi-NPP VIIRS due to surface roughness-induced Rayleigh scattering," *Remote Sens.* **8**(3), 254 (2016).
21. J. Sun and M. Wang, "Radiometric calibration of the Visible Infrared Imaging Radiometer Suite reflective solar bands with robust characterizations and hybrid calibration coefficients," *Appl. Opt.* **54**(31), 9331–9342 (2015).
22. S. Mills et al., "Calibration of the VIIRS day/night band (DNB)," in *American Meteorological Society 6th Annual Symp. Future National Operational Environmental Satellite Systems-NPOESS and GOES-R* Vol. **9** (2010).
23. NOAA/NESDIS/STAR, "GOES ABI Calibration Events Log," https://www.star.nesdis.noaa.gov/GOESCal/goes_SatelliteAnomalies.php (2019).
24. R. Morfitt et al., "Landsat-8 operational land imager (OLI) radiometric performance on-orbit," *Remote Sens.* **7**(2), 2208–2237 (2015).
25. P. Minnis et al., "Assessment of the visible channel calibrations of the VIRS on TRMM and MODIS on aqua and terra," *J. Atmos. Oceanic Technol.* **25**(3), 385–400 (2008).
26. P. Minnis et al., "Rapid calibration of operational and research meteorological satellite imagers. Part I: evaluation of research satellite visible channels as references," *J. Atmos. Oceanic Technol.* **19**(9), 1233–1249 (2002).
27. D. R. Doelling et al., "Algorithm theoretical basis document (ATBD) for ray-matching technique of calibrating GEO sensors with aqua-MODIS for GSICS," NASA-Langley SSAI (2011).
28. National Calibration Center, NESDIS/STAR, "SNPP SNOs with other satellites," https://ncc.nesdis.noaa.gov/VIIRS/SNOPredictions/index.php (2019).

29. C. Cao, M. Weinreb, and H. Xu, "Predicting simultaneous nadir overpasses among polar-orbiting meteorological satellites for the intersatellite calibration of radiometers," *J. Atmos. Oceanic Technol.* **21**(4), 537–542 (2004).
30. NOAA, The Comprehensive Large Array-data Stewardship System (CLASS), "VIIRS_SDR," https://www.avl.class.noaa.gov/ (2020).
31. NASA, "Spectral band adjustment factor (SBAF) calculator based on SCIAMACHY visible hyperspectral data," https://satcorps.larc.nasa.gov/cgi-bin/site/showdoc?mnemonic=SBAF (2018).
32. B. R. Scarino et al., A web-based tool for calculating spectral band difference adjustment factors derived from SCIAMACHY hyperspectral data," *IEEE Trans. Geosci. Remote Sens.* **54**(5), 2529–2542 (2016).
33. D. L. Helder et al., "Updated radiometric calibration for the Landsat-5 Thematic Mapper reflective bands," *IEEE Trans. Geosci. Remote Sens.* **46**(10), 3309–3325 (2008).
34. B. L. Markham et al., "Landsat-7 ETM+ on-orbit reflective-band radiometric stability and absolute calibration," *IEEE Trans. Geosci. Remote Sens.* **42**(12), 2810–2820 (2004).
35. B. L. Markham and D. L. Helder, "Forty-year calibrated record of earth-reflected radiance from Landsat: a review," *Remote Sens. Environ.* **122**, 30–40 (2012).
36. NOAA/NESDIS/STAR, GOES Calibration,, "GOES ABI calibration events log," https://www.star.nesdis.noaa.gov/GOESCal/goes_SatelliteAnomalies.php (2020).
37. X. Shao et al., "Validation of GOES-16 ABI reflective solar band calibration through reanalysis and comparison with field campaign data," *Proc. SPIE* **10764**, 107640I (2018).

Sirish Uprety received his MS degree in electrical engineering from South Dakota State University, USA, in 2009. He is a member of the Visible Infrared Imaging Radiometer Suite (VIIRS) calibration/validation support team at CISESS, University of Maryland, College Park, USA. He is primarily working on the postlaunch calibration and validation of VIIRS onboard S-NPP and NOAA-20 satellites. He has worked on a wide range of satellite instruments that includes the Earth observing multispectral and hyperspectral sensors.

Changyong Cao received his BS degree from Peking University, China, in 1982 and PhD in geography from Louisiana State University, USA, in 1992. He serves as a research physical scientist with the NOAA/NESDIS/STAR, College Park, Maryland, USA, since 1999 and specializes in the calibration/validation of radiometers onboard NOAA's Operational Environmental Satellites, where he leads the VIIRS Sensor Science Team. He received two gold medals and one silver medal from the U.S. Department of Commerce.

Xi Shao received his BS degree in physics from the University of Science and Technology of China, China, in 1996, PhD in astronomy, and MS degree in EE from the University of Maryland, USA, in 2004. He is an associate research scientist with the Department of Astronomy and Cooperative Institute for Climate and Satellites, the University of Maryland. He supports radiometric calibration/validation of Visible Infrared Imaging Radiometer Suite (VIIRS) instrument and Advanced Baseline Imager (ABI) onboard NOAA satellites.